ELSEVIER

Contents lists available at ScienceDirect

Biomaterials Advances

journal homepage: www.journals.elsevier.com/materials-science-and-engineering-c





3D printing of thick myocardial tissue constructs with anisotropic myofibers and perfusable vascular channels

Haitao Cui ^{a,b}, Zu-Xi Yu ^c, Yimin Huang ^c, Sung Yun Hann ^b, Timothy Esworthy ^b, Yin-Lin Shen ^b, Lijie Grace Zhang ^{b,d,e,f,*}

- a Key Laboratory of Biorheological Science and Technology, Ministry of Education, College of Bioengineering, Chongqing University, Chongqing, 400044, China
- b Department of Mechanical and Aerospace Engineering, The George Washington University, Washington, DC 20052, United States of America
- ^c National Heart, Lung, and Blood Institute, National Institutes of Health, Bethesda, MD 20892, United States of America
- d Departments of Electrical and Computer Engineering, The George Washington University, Washington, DC 20052, United States of America
- e Department of Biomedical Engineering, The George Washington University, Washington, DC 20052, United States of America
- f Department of Medicine, The George Washington University, Washington, DC 20052, United States of America

ARTICLE INFO

Keywords: 3D printing Vasculature Decellularized extracellular matrix Thick myocardial tissue Myocardial infarction

ABSTRACT

Engineering of myocardial tissues has become a promising therapeutic strategy for treating myocardial infarction (MI). However, a significant challenge remains in generating clinically relevant myocardial tissues that possess native microstructural characteristics and fulfill the requirements for implantation within the human body. In this study, a thick 3D myocardial construct with anisotropic myofibers and perfusable branched vascular channels is created with clinically relevant dimensions using a customized beam-scanning stereolithography printing technique. To obtain tissue-specific matrix niches, a decellularized extracellular matrix microfiber-reinforced gelatin-based bioink is developed. The bioink plays a crucial role in facilitating the precise manufacturing of a hierarchical microstructure, enabling us to better replicate the physiological characteristics of the native myocardial tissue matrix in terms of structure, biomechanics, and bioactivity. Through the integration of the tailored bioink with our printing method, we demonstrate a biomimetic architecture, appropriate biomechanical properties, vascularization, and improved functionality of induced pluripotent stem cell-derived cardiomyocytes in the thick tissue construct in vitro. This work not only offers a novel and effective means to generate biomimetic heart tissue in vitro for the treatment of MI, but also introduces a potential methodology for creating clinically relevant tissue products to aid in other complex tissue/organ regeneration and disease model applications.

1. Introduction

Myocardial infarction (MI) is the major cause of mortality associated with cardiovascular diseases, accounting for an estimated 18 million deaths annually and 23 % of all deaths worldwide, in accordance with the World Health Organization's statistics report in 2022 [1]. Medications, angioplasty, and bypass graft surgery are the current standard treatments in clinical use to treat MI [2]. Due to the poor regenerative capacity of adult cardiac muscle, current treatments only relieve the symptoms of MI, but fail to repair necrotic heart tissues and restore their functionality [3]. As such, the engineering of cardiac tissues has become a promising therapeutic method to repair the damaged myocardium for MI treatment [4–7].

Many studies have shown that cellularized cardiac patches/constructs which combine stem cells, biomaterials, and bioengineering strategies can prevent post-infarction remodeling and repair the damaged myocardium [8–10]. For example, an heart tissue strip was created by the combination of human induced pluripotent stem cell-derived cardiomyocytes (hiPSC-CMs) and endothelial cells, which was implanted onto damaged large heart tissue of guinea pigs [11]. Results showed that engineered human heart muscle constructs could repair the injured heart of the guinea pig. Additionally, a micro-vascularized cardiac patch (\sim 100 μ m in thickness) was created to imitate the structural dimensions and protein composition of the myocardium to improve cardiac function after MI [12]. They mentioned that creating cardiac patches with sufficient size for large animal studies would be their

^{*} Corresponding author at: Science and Engineering Hall 3590 800 22nd Street NW, Washington, DC 20052, United States of America. E-mail address: lgzhang@gwu.edu (L.G. Zhang).

subsequent work. Recently, a cardiac patch (~ 1.5 mm in thickness) comprised of decellularized matrix and synthetic cells was developed to test its therapeutic effect in vivo, but it was still limited by the sample size in the implantation study of pig models as they discussed [13]. In our previous studies, a series of thin cardiac patches (≤1 mm in thickness) have also been developed for MI treatment [14-16]. Study results have demonstrated the advantages of utilizing constructs that feature anisotropically patterned myofibers and vascularization [14,15], which effectively increase cell engraftment and vascular supply within an in vivo animal study [14]. However, these thin patches/constructs generally lack clinically relevant dimensions and perfusable vessels to efficiently transport nutrients/oxygen to satisfy the demand for the repair of large, thick human MI-damaged myocardium. Therefore, a considerable challenge in engineering cardiac tissues is to replicate the complex architecture and biological functions at clinically relevant dimensions, including thick anisotropic myofibers and perfusable branched vasculature networks [17,18].

3D printing offers an effective means to create complicated architectures with hierarchical macro/micro features at clinically-relevant large dimensions for engineering tissues/organs [19-23]. Recently, the 3D printing approach has been successfully employed to fabricate various perfusable complex tissues, such as blood vessels [24-26], vascularized bone [27-29], and vascularized cancer models [30]. Although 3D printing exhibits its capability in the fabrication of large dimensional tissue products, extrusion printing is difficult to independently achieve the hierarchical multiscale micromanufacturing of tissue constructs due to the limitation of ink viscosity and printing resolution. Therefore, the previous studies have yet to replicate the anisotropic myofibers and perfusable branched vasculature of native myocardial tissue at clinically relevant dimensions. Our customized beam-scanning stereolithography (SL) printing, a type of vat photopolymerization, has exhibited a distinct advantage in its capacity to precisely manufacture tissue constructs with photocrosslinkable inks at high speed, high resolution, and high reproducibility. The printing speed and laser intensity can be adjusted to tailor the crosslinking degree of the hydrogels, in turn affecting the physicochemical properties of tissue constructs [30-32]. Therefore, in comparison to extrusion or other printing techniques, SL printing exhibits the greatest potential to replicate the structural and mechanical complexity of the native tissue at clinically relevant dimensions [19,33]. However, the drawback of SL printing is overexposure and multiexposure, which easily leads to the failure of the fabrication of the opening channels and/or pores in the vertical direction.

In addition to architectural and mechanical considerations that need to be made in designing complex structures, the ink materials (biomaterials or other components) used in printing also play crucial roles in the biomechanics and bioactivity of tissue constructs, and thus need to be tailored accordingly [21,34,35]. Biomaterials derived from or partially based on natural sources have the potential to create a more conducive environment for cellular growth. For example, decellularized extracellular matrix (dECM) of tissues/organs can effectively preserve the fibrous protein (e.g., COL), glycoproteins (e.g., glycosaminoglycans (GAGs)), signaling molecules (e.g., growth factors) and other matrix components (e.g., receptors) in native tissues, providing biological cues for the repair and regeneration of damaged tissues [36,37]. Therein, dECM can confer synergistic biochemical and biomechanical signaling effects towards supporting tissue regeneration [36,38]. Currently, dECM bioinks of animal-derived cardiac tissues have been used in 3D printing myocardial tissues for cardiac regeneration [9,39-41]. In previous studies, dECM bioinks are generally prepared through pepsin (proteinase) solubilization to make them extrudable [29,30]. Instead of being digested in the pepsin solution for extrusion printing, dECM microfibers can be dispersed into the photocrosslinkable ink in SL printing, which maintains the 3D fibrous microstructure and bioactivity of the native ECM, and enhances the mechanical properties of printed hydrogels. More importantly, the addition of dECM microfibers can affect light transmission to weaken the photon absorption of photocrosslinkable

bioink in SL printing, potentially contributing to the successful fabrication of the opening channels/pores in the vertical direction.

In this study, a novel thick myocardial construct (~5 mm in thickness) has been developed with anisotropic myocardial fibers and a perfusable branched vasculature using a dECM microfiber-reinforced photocrosslinkable bioink and SL printing technique towards the goal of healing MI-damaged heart tissue within human beings postimplantation. The hiPSC-CMs are demonstrated as a promising cell candidate for myocardial regeneration and clinical translation [42]. iPSCs are derived directly from adult cells through gene reprogramming and can readily differentiate into cardiomyocytes, which can overcome the difficulties in cell sources and avoid controversial ethical issues [4,43,44]. To mimic the native microenvironment, a dual biomechanical stimulation was utilized, which integrates dynamic flow stress and mechanical loading to improve the cellular functionalities of regenerated thick cardiac tissue. It is expected that the re-establishment of anisotropic myofibers and blood circulation at clinically relevant dimensions can effectively replicate the structural specificity and environmental complexity of the native myocardium. This will not only aid in furthering our understanding of the physiological process of cardiac tissue repair and regeneration, but will also potentially provide an effective method to repair MI-damaged myocardial tissues in adult

2. Materials and methods

2.1. Materials

All chemicals were purchased from Sigma-Aldrich. They were used as received without any further process. All materials used for cell experiments were sterilized before use.

2.2. Preparation of dECM fibers of myocardial tissue

A porcine heart was collected from an 8-month-old domestic pig (obtained from a local butcher). The left ventricular free wall was cut and decellularized using the following method. After minced with a meat grinder (equipped with a 1 mm cutting plate), myocardial tissues were stirred with sodium dodecyl sulfate solution (1 wt%) for 48 h, and then treated with Triton X-100 solution (1 wt%) for 1 h. After which, in order to remove residual detergent, the dECM was washed with phosphate-buffered saline (PBS) (every 8 h for each change) for 3-5 days. The dECM was then sterilized using an antibiotic-antimycotic solution (Corning) for 24 h, followed by rinsing three times with sterilized PBS. Finally, the dECM was lyophilized and subsequently pulverized to microfibers using a blender under sterile conditions. To obtain the uniform distribution of microfibers, the dECM microfibers were sieved through lab sieves of a 350 µm mesh and a 450 µm mesh under sterile conditions. The resulting monodispersed dECM microfibers were stored in a -20 °C freezer prior to use. The relative weight ratio of lyophilized (dry) tissue and dECM was measured, where the fresh tissue was set to 100 % as a standard control.

2.3. Preparation of dECM microfiber-reinforced photocrosslinkable inks

Gelatin Type A (10 g) was dissolved in pure water at 80 °C. Methacrylic anhydride (5 mL) was added and reacted at 80 °C for 3 h. The resulting gelatin methacrylate (GelMA) was dialyzed in pure water at 40 °C for 5 days. Finally, the GelMA solution was lyophilized to obtain a solid white product. In accordance with our previous study [14], the photocrosslinkable ink solution with the optimized formulation that was used for the present study was prepared using PBS solution consisting of 5 wt% GelMA, polyethylene glycol diacrylate (PEGDA) (Mn = 700; 5, 10, and 15 wt%), and 1 wt% photoinitiator Irgacure 2959. Then ink solutions with different amounts of dECM microfibers (1 %, 3 %, 5 %, 7 %, and 10 %) were prepared to obtain the dECM reinforced GelMA/

PEGDA (dECM@GP) bioinks for the study experiments, while the GelMA/PEGDA (GP) ink was served as the study control. Before conducting other experiments, the pH of all ink solutions was adjusted to 7.4, and the inks were vigorously shaken for 2 h, allowing for the complete swelling and homogeneous dispersion of microfibers in the inks.

2.4. CAD design and SL printing of thick cardiac constructs

A thick cardiac construct was designed with clinically relevant dimensions (size ≥ 2 cm \times 2 cm, and thickness ~ 5 mm, according to the data from references [18, 45]) using the Rhinoceros 4.0 3D imaging package to replicate the complex architecture (anisotropic myocardial fibers and branched perfusable vasculature) of the native cardiac tissue. In accordance with our previous study [14], a wave-like (or hexagonal) microstructure was designed to mimic the fiber orientation of the native myocardium. The pattern with a 200 μm width was printed with 40 %fill density to stack at an angle of 45° for adjacent layers [14]. Additionally, the branched vasculature with 1 mm perfusable channels in diameter was designed to be embedded into the printed myofibers of the cardiac tissue. The CAD construct model (.stl) was processed with Sli3er and predicted for structural characteristics. The thick cardiac constructs were fabricated using our customized beam-scanning SL printer. The SL printer was built on the Printrbot prototyping platform with three-axis motion, which consists of a movable stage with an ink reservoir and an X-Y toolhead with a 110 µm UV laser fiber (355 nm). The speed of SL printing was maintained at 1 cm/s. The laser intensity was set at 20 kHz (an energy output of $\sim 20 \,\mu$ J). Based on our previous studies [14,30,32], these parameters could ensure high printing resolution, structural stability, and cell viability.

2.5. Biochemical characterization of dECM@GP hydrogel

The residual DNA was measured to assess the quality of the myocardial decellularization, and the content of COL and sulfated GAGs was also assessed to evaluate the matrix components in the dECM microfibers and dECM@GP hydrogels. To quantify residual DNA, 100 mg fresh tissue (control), resultant dECM microfibers, and hydrogels were triturated in 1 mL Trizol (Invitrogen) using a homogenizer. The DNA pellet was collected based on the manufacturer's protocol. The content of double-stranded DNA (ds DNA) was measured using a QuantiT Picogreen® dsDNA assay kit (Invitrogen). The Quant-iT Picogreen®reagent was added to the DNA Tris-EDTA buffer solution, and then incubated for 5 min. The fluorescence was measured by an H1 microplate reader (Hybrid Technology) at 480/520 nm.

To assess the constituent component of the dECM, the amounts of COL and sulfated GAGs in the fresh tissue (control), dECM microfibers, and resultant hydrogels were measured. The solubilized collagen was extracted with 0.2 % pepsin/acetic acid for 48 h at 4 °C, and then quantified using a Picro Sirius red dye assay. The suspension was dried at 60 °C overnight, and then treated with 0.1 % Sirius red/picric acid solution for 1 h. The precipitate of each wall was rinsed with 5 % acetic acid and PBS three times. Finally, the precipitate was dissolved in 0.1 M NaOH solution. The collagen content (optical density, OD) was determined using a Multiskan GO Microplate Spectrophotometer (Thermo Fisher) at 555 nm, and collagen standards were compared to calculate the content. The GAG content (OD) was assessed using a dimethyl methylene blue (DMB) assay. Sulfated GAGs were extracted with a papain digestion solution (1 mg/10 mL buffer) for 12 h at 65 $^{\circ}$ C. The digested samples were supplemented with DMB solution (1/10, v/v). Samples were shaken for 10 s, and then the OD value at 525 nm was immediately measured with a spectrophotometer. The chondroitin sulfate was used to obtain a standard curve, and the GAG levels of samples were calculated accordingly.

2.6. Characterization

The printability of the study SL printing system was evaluated by the transmission of UV light in the different inks, and the OD value at 650 nm was measured with a spectrophotometer. The mean trajectory error (Et) was used to evaluate the structural accuracy post-printing using a previously described method [14]. The swelling profile of the printed samples was quantified by the relative weight change. After being immersed in PBS for 7 days at 37 °C, the weight changes of printed constructs were calculated as $(w_f - w_o)/w_o \times 100$ %, where w_o represents the original weight, and w_f represents the final weight after equilibrium swelling. The water absorption after equilibrium swelling was measured by the weight change of dried hydrogel constructs. The water absorption ratios of constructs were calculated as $(w_f-w_d)/w_d \times 100$ %, where w_d represents the weight of dried samples, and $w_{\rm f}$ represents the final weight. Additionally, tensile and compressive moduli were tested using a 100 N load MTS criterion universal system (MTS Corporation). In compression testing, samples were compressed with a preload of 0.01 N at a strain rate of 2 mm/min to a strain of 20 %; and in tension testing, the samples were pulled at a rate of 1 mm/min to a strain of 20 %. Young's moduli of the samples were obtained from the slope of the linear part of the stress-strain curves.

2.7. Cell culture

hiPSC-CMs were cultured according to the previously reported protocol [46]. Both hiPSC-CMs and cardiomyocyte basic medium were obtained from iPSC Core at the NHLBI. The cardiomyocyte basic medium consisted of E8 basal medium (including DMEM/F-12, selenium, transferrin, L-ascorbic acid, and NaHCO₃), 1 % Chemically Defined Lipid Concentrate (ThermoFisher Scientific), 20 μ g/mL insulin and 1 % penicillin/streptomycin. Human (umbilical vein) endothelial cells (hECs) at six cell passages or less (ThermoFisher Scientific) were cultured in EGMTM-2 medium (Lonza). And human (bone marrow) mesenchymal stem cells (hMSCs) at six cell passages or less (Texas A&M Health Science Center) were cultured in MSC medium (alpha minimum essential medium, 1 % penicillin/streptomycin 1 % L-glutamine, and 20 % fetal bovine serum). Cell experiments were performed in an incubator with a humidified, 37 °C, and 5 % CO₂ environment.

2.8. In vitro culture of cellularized cardiac constructs

According to our previous study on microvascularized cardiac patches [14], hiPSC-CMs, hECs, and hMSCs were seeded with a ratio of 4:2:1 to produce the resultant cellular proportion (3:4:3) similar to the cellular composition of human myocardial tissue [47,48]. Similarly, the mixed cells (2 \times 10⁵ cells/cm²) were seeded into the myocardial fiber area of our thick constructs, and the cell/medium suspension was injected multiple times into the different positions in order to obtain a uniform distribution. Besides, in order to create the endothelialized large vessels in this study, hECs (5 \times 10³ cells/ μ L) were perfused into open vascular channels (500 µL of hEC suspension was injected via pipette to fill the vascular channels, and after each 30 min, the constructs were flipped to improve cell adhesion around channels' inner surface). After 3 h, the constructs were tri-cultured in the mixed (1:1:1) medium. To visualize the cell distribution in the constructs, hiPSC-CMs, hMSCs, and hECs were stained in green, blue and red colors with Cell-Tracker™ dyes, respectively (Molecular Probes). Cells within constructs were imaged via a Zeiss 710 confocal microscope after 7 days of coculture. The cell proliferation profiles of cells growing on the hydrogel construct with a mono-culture method composed of different ink formulations for up to 7 days were quantitively assessed using a CCK-8 kit (Dojindo). The cell proliferation of cells (OD) was measured using the spectrophotometer at 570 and 600 nm after 2 h of incubation. After 7 days of culture, the constructs were fixed for 30 min using formalin solution, and permeabilized for 20 min using 0.1 % Triton X-100

solution. Then cellular spreading morphology was studied using the Factin staining (Texas Red-X Phalloidin, 1:200), while nuclei were stained with DAPI (4, 6-diamidino-2-phenylindole dihydrochloride, 1:1000) (Thermo Scientific). Cells were imaged via the confocal microscope. Moreover, in order to compare the functional beating of hiPSC-CMs on the 2D well plate and 3D constructs, after 5 and 10 days of culture, the contractile behavior of iPSC-CMs was observed via microscope, and then the contraction rate (beat per minute, BPM) was calculated.

2.9. Dual biomechanical stimulation in a customized bioreactor system

Our thick constructs were incubated in a customized bioreactor system for 2 weeks, which consisted of (1) a dynamic flow device (the tissue constructs were perfused with the medium, facilitating the efficient supply of oxygen and nutrients) to produce dynamic flow-induced shear stresses and (2) a mechanical loading device (the constructs were mounted by a PDMS holder in a polymethylmethacrylate chamber for transferring the mechanical loading and preventing undesired movement and damage). A shear stress of 15 dyn/cm² within the range of in vivo shear stress was yielded by applying a flow rate of 12.6 mL/min [24,49]. The preload contractile force of ~50 mN/mm² was yielded along the constructs' fiber direction at a speed of 60 reps/min in the radial direction by a piston pressure to match the mechanical values of the native cardiac tissue.

2.10. Cell immunostaining

Cellular functions (i.e., cardiomyogenesis and angiogenesis) were evaluated by immunofluorescent staining. After 2 weeks of culture, our constructs were fixed for 30 min using a formalin solution. Additionally, sliced fragments of constructs (5–10 μm) were also assessed to observe the inner cross-sectional performance. The samples were permeabilized for 20 min using 0.1 % Triton X-100 solution, followed by blocking for 6 h in a 1 % bovine serum albumin solution with 0.3 M glycine and 0.1 % Tween 20. After which, the constructs were incubated in the primary antibodies overnight at 4 °C. Then secondary antibodies were used to color cells in the dark for 2 h. Finally, the samples were counterstained with DAPI (1:1000) for 10 min, and then images were taken by a confocal microscope. The primary antibodies included anti- α -actinin (sarcomeric alpha-actinin, 1:500 (ab137346)), anti-CD31, 1:500 (ab9498)), anti-cTnI (cardiac troponin I, 1:500 (ab38210)), and antivWf (von Willebrand factor, 1:1000 (ab6994)) (Abcam). Anti-mouse Alexa Fluor 594 and goat anti-rabbit Alexa Fluor 488 (1:1000) were used as the secondary antibodies (Thermo Scientific).

2.11. Histological examination

The dECMs or constructs were fixed in formalin solution, and processed in 5 % sucrose solution. The samples were embedded with cutting temperature compound, and then cut into 5–10 μm slices for the cryosection study. Hematoxylin-eosin (H&E) staining was performed to analyze the structure of the dECMs or constructs and the corresponding cellular distributions.

2.12. Gene expression analysis

An rt-PCR (reverse transcription-polymerase chain reaction) assay was conducted to evaluate the cardiac tissue-related gene expression in accordance with the manufacturer's protocol. Briefly, the RNA was extracted with Trizol reagent, and the purity and concentration of RNA were tested by a microplate reader. cDNA was synthesized with a Prime Script™RT Kit, and rt-PCR was conducted with SYBR Premix Ex Taq™ Kit (TaKaRa) using a CFX384 Real-Time System (BIORAD). Cardiac troponin I (TNNI3), ryanodine receptor 2 (RYR2), myosin light chain 7 (MYL7), and platelet/endothelial cell adhesion molecule-1 (PECAM1)

were analyzed to assess the functionality of cardiac cells. The relative gene expression was normalized against the control group (GP hydrogel) and the gene expression levels were normalized against glyceraldehyde 3-phosphate dehydrogenase (GAPDH). The primers are shown in Table 1 [12].

2.13. Statistical analysis

The experiments were repeated a minimum of three times. The sample sizes in each independent experiment have been shown in the figure captions. All data are expressed as the mean \pm standard deviation (SD). To determine significant differences, a one-way analysis of variance (ANOVA) with Tukey's test was performed using Origin Pro 8.5 (*p < 0.05, **p < 0.01, and ***p < 0.001).

3. Results and discussion

To obtain the myocardial tissue-specific bioinks and hydrogel constructs, the native myocardial dECM fibers were mixed with photocrosslinkable GelMA and PEGDA ink solutions (Fig. 1a). As a molecular derivative of gelatin (COL hydrolysate), GelMA is a well-characterized photocrosslinkable biomaterial that is suitable for SL printing, and has been shown to provide bioactivity and mechanical tunability to support cell adhesion and growth. However, the high swelling volume of pure GelMA hydrogel significantly affects the structural stability and fidelity of the printed constructs, which cannot be avoided by increasing light exposure or GelMA concentration. The addition of PEGDA in the ink formulation effectively increases the crosslinking degree of printed hydrogels, while simultaneously decreasing the bulk swelling volume, increasing the mechanical strength, enhancing the printing fidelity, and improving the structural stability [14]. Moreover, to recapitulate the tissue-specific matrix niche needed for the restoration of cellular functionality, the dECM fibers of the porcine left ventricle were prepared using an optimized decellularization protocol (Fig. 1b). Photo images also showed the white micro-fibrous powder was successfully prepared to yield a hybrid hydrogel (disc) with an extensive distribution of dECM fibers. The shape of hydrogel constructs could be changed based on the design and fabrication. The H&E staining results of dECM also illustrated that the decellularization process sufficiently removed all cytological components (without blue-colored nuclei) while preserving the densely striated and fibrous (COL, pink color) structure of the native ECM [40,50], as shown in Fig. 1c. Fig. 1d shows the dECM retained >80 wt% of the dry myocardial tissue post-decellularization, suggesting the high efficiency of the matrix preservation. Quantitative assessment of the dsDNA demonstrated a significant decrease in residual DNA of dECM fibers, and the value was similar to that of other studies [40,50], further confirming the success of the decellularization process (Fig. 1e). Moreover, a significant reduction in the COL or sulfated GAGs content of the dECM fibers was not observed compared to their respective content within the native tissue control, further indicating that the removal of cytological components and purification of the dECM conferred a minimal loss of these functional components through the processing procedures (Fig. 1f and g). In general, similar to other decellularization studies, the decellularization process preserved the structural characteristics and major components of the ECM fibers.

As discussed above, the dECM fibers was homogeneously dispersed into photocrosslinkable GP bioink to obtain a series of dECM@GP bioinks with the ratios of 1, 3, 5, 7, and 10 wt%. It was found the ink with 7 wt% dECM fibers was too viscous to flow, and a congealed gel was formed using the ink with 10 wt% dECM fibers. Additionally, as a prerequisite for SL printing, inks must permit the penetration of emitted UV light. Thus, it was found that the printing ability of the resulting dECM fiber-doped ink solutions was light transmittance-dependent due to the dissolution of opaque dECM fibers (Fig. 2a). As we hypothesized above, it was found that the limited light transmission could avoid overexposure and multiexposure to achieve more precise manufacturing,

Table 1Primers of quantitative rt-PCR.

Gene name	Protein name	Forward primer	Reverse primer	Size bp
GAPDH	GAPDH	GGAGCGAGATCCCTCCAAA	GGCTCCCCCTGCAAA	115
TNNI3	cTNI	CCTCACTGACCCTCCAAACG	GAGGTTCCCTAGCCGCATC	104
RYR2	RYR2	TTGGAAGTGGACTCCAAGAAA	CGAAGACGAGATCCAGTTCC	141
MYL7	MLC 2a	GGAGTTCAAAGAAGCCTTCAGC	AAAGAGCGTGAGGAAGACGG	178
PECAM1	CD31	GAGTCCTGCTGACCCTTCTG	CACTCCTTCCACCAACACCT	175

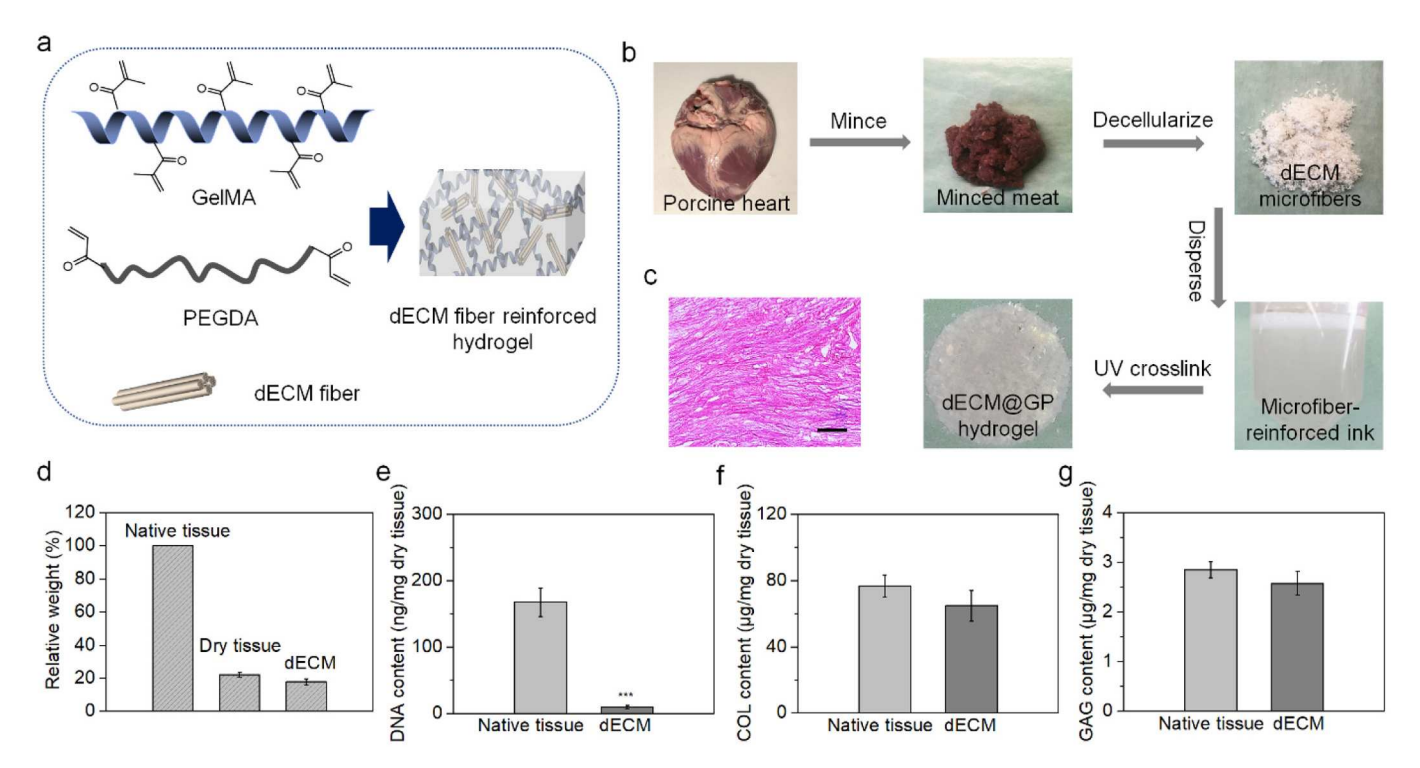


Fig. 1. Preparation of dECM fibers and dECM fiber-reinforced hydrogel. (a) Schematic illustration of the bioink composition and hydrogel. (b) Decellularization of the myocardial tissue and preparation of the resultant hydrogel (disc as an example). (c) Histological (H&E) image of the dECM, illustrating the retention of native fiber features and the complete removal of cells. Scale bar, 100 μ m. (d) The relative weight percentage of the dECM fibers post-decellularization compared to the fresh tissue and the lyophilized tissue (means \pm SD, $n \ge 9$). (e) Residual dsDNA content of the native tissue and the dECM fibers (means \pm SD, $n \ge 6$, ***p < 0.001). (f) COL content and (g) GAG content in the ECM components and the dECM fibers compared to their respective content within the native tissue control (means \pm SD, $n \ge 6$, no significant difference).

especially in the vertical direction. It would be beneficial for the generation of our perfusable (opening) vascular channels within the thick cardiac construct. Furthermore, the SL printing accuracy of the different inks was further investigated. The results demonstrated that the inks with lower than 3 wt% dECM fibers were relatively acceptable for around 80 % print fidelity, as shown in Fig. 2b. Fig. 2c shows the photo image and microscopic image of the printed hydrogel, which illustrates the morphology of dECM fibers in the hydrogel and the porous structure of the printed hydrogel. The cross-sectional image of the H&E stained hydrogel construct shows the distribution of extensive dECM fibers (COL, red) within the microarchitecture (mesh, purple) of the printed construct (Fig. 2d), although the general homogeneity of the fibers in the constructs is difficult to illustrate due to the limitation of slide thickness (\sim 5 μ m). As shown in Fig. 2e, SEM images illustrated the significant difference in surface morphology between GP and dECM@GP hydrogels, confirming the presence of dECM fibers in the dECM@GP hydrogel. To quantitatively study the ECM components in the printed hydrogels, COL and sulfated GAGs content in the different dECM@GP hydrogels were measured (Fig. 2f and g). The results showed an increased concentration of COL and sulfated GAGs with an increasing amount of dECM fibers.

Next, the relative weight change of different dECM@GP hydrogels after equilibrium swelling was further studied. As shown in Fig. 2h, the

weights of the hydrogels were greatly increased by increasing the ratio of dECM fiber content to the GP ink base, which attributed to the significant swelling of dECM fibers. A slight decrease in initial weight was observed due to the partial loss of unfixed dECM fibers in the hydrogel. According to the results of our previous study [14], the GP ink formulations with the concentrations of 5 % GelMA and (5, 10, and 15 %) PEGDA were optimized to obtain physiologically relevant mechanical behaviors. To better analyze the role of the dECM fibers in the printed hydrogels, we also tested the physical properties of the printed hydrogels with varying ratios of dECM fibers and the concentrations of PEGDA. Similar to the swelling profiles, the rise in the ratio of dECM fibers led to an increase in water absorption (Fig. 2i). Meanwhile, the increase of PEGDA contents significantly decreased the swelling behavior of the dECM fibers in the hydrogels. This observation can be best explained by the dense network space of the highly crosslinked hydrogels hindering the water absorption capacity of the dECM fibers. Moreover, although the concentration of PEGDA played a significant role in the mechanical strength of the photocrosslinked GP hydrogels, we also observed that the amount of dECM fibers largely affected the mechanical modulus of the resulting hydrogels (Fig. 2j and k). It was demonstrated that the tensile moduli of the dECM fiber-reinforced hydrogels with 5 % GelMA and 10 % PEGDA matched the matrix

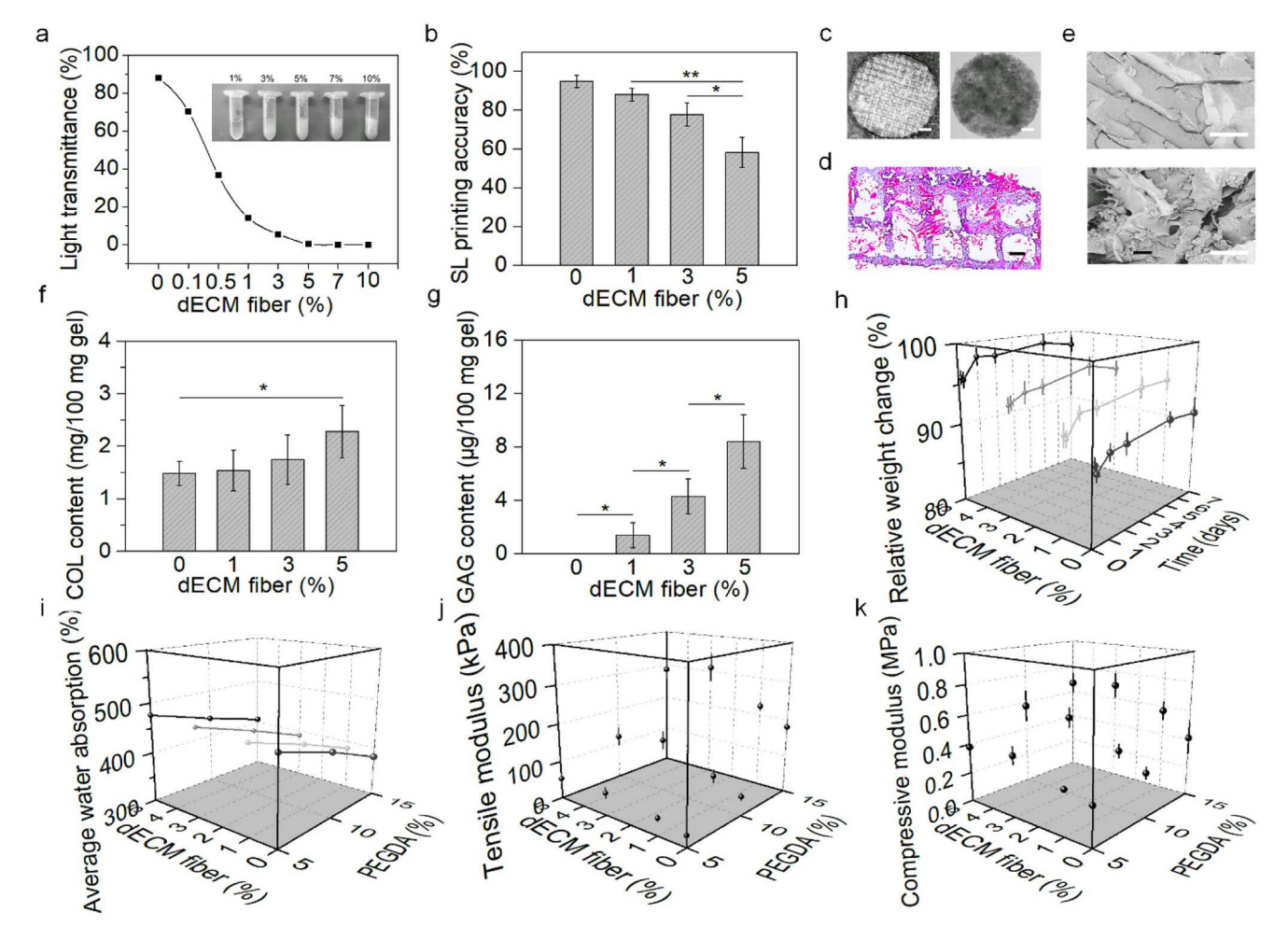


Fig. 2. Characterization of the 3D printed dECM fiber-reinforced hydrogels. (a) SL printability of dECM@GP bioinks with different ratios of the dECM fibers. (b) Printing accuracy of the hydrogel constructs using the bioinks with different ratios of the dECM fibers (means \pm SD, $n \ge 6$, **p < 0.01, and *p < 0.05). (c) Photo image (left) and microscopic image (right) of the 3D printed hydrogels. Scale bar, 1 mm. (d) Cross-sectionally histological (H&E) image of the dECM fiber reinforced hydrogel, showing the distribution of extensive dECM fibers within the microarchitecture of the printed hydrogel. Scale bar, 200 μ m. (e) SEM images of the GP (top) and dECM@GP (bottom) hydrogels, confirming the presence of dECM fibers in the hydrogel. Scale bar, 100 μ m. (f) COL content and (g) GAG content in the dECM@GP hydrogels with different ratios of the dECM fibers (means \pm SD, $n \ge 6$, *p < 0.05). (h) Relative weight change of dECM@GP hydrogels with varying ratios of the dECM fibers and PEGDA. (j) Tensile modulus of dECM@GP hydrogels with varying ratios of the dECM fibers and PEGDA (means \pm SD, $n \ge 6$). (k) Compressive modulus of dECM@GP hydrogels with varying ratios of the dECM fibers and PEGDA (means \pm SD, $n \ge 6$). (k) Compressive

modulus of the native myocardium ($\approx 10^1$ – 10^2 kPa) [51,52]. With consideration for the optimized printability, hydrogel elasticity, and potential bioactivity of dECM, the bioink comprised of 5 wt% GelMA, 10 wt% PEGDA, and 3 wt% dECM fibers was used to fabricate the myocardial constructs. Moreover, the printed constructs maintained the fibrous structure of native ECM while displaying enhanced mechanical moduli and bioactivity. The properties of the tissue microenvironment determine the cellular function and fate; therefore, it is expected that the dECM fiber-reinforced hydrogels from myocardial-specific tissue would support and improve the growth and functionality of the resident cells.

Within the native heart, a helical network of myofibers surrounded by collagen sheaths is organized into a thick-walled ventricle, yielding directionally dependent (anisotropic) electromechanical properties [53,54], while the large and perfusable cardiac vasculature efficiently transports oxygen, nutrients, and waste, which is critical for supporting the metabolic activity of cardiac tissue, which cannot be obtained via capillary-based pre-vascularization [55,56] (Fig. 3a). Therefore, we designed and developed a thick cardiac tissue construct with anisotropic myofibers and branched perfusable vasculature with clinically relevant dimensions (size $\sim\!\!2\times\!2$ cm and thickness $\sim\!\!5$ mm) to replicate the native characteristics of the human heart towards the goal of repairing

post-MI-damaged human myocardial tissue and restoring its functionality. In our previous work [14], as compared to other anisotropic patterns, the hexagonal infill printing pattern has been shown to generate a highly stretchable structure with minimal hydrogel deformation to avoid material fatigue under cyclic loading, although the anisotropy of thick constructs was difficult to characterize in this study. Fig. 3b shows a 3D-printed thick cardiac tissue construct fabricated using the dECM@GP bioink, and Fig. 3c shows the cellularized cardiac tissue construct with cocultured hiPSC-CMs, hECs, and hMSCs over one week. Similar to cardiac fibroblasts, the hMSCs were used as supportive cells to enhance the organization of regenerated cardiac tissue. The essential process to generate a functional tissue involves allowing the encapsulated cells to grow, aggregate, and produce newly secreted ECM. It was observed that the cardiac construct had an obvious change of morphology due to its cellularization process after 7 days of culture.

Fluorescent images (Fig. 3d and e) illustrate the hexagon patterned myofibers with hiPSC-CMs and a (half) hollow channel of the endothelialized vessel with hECs. After 7 days of coculture, it was observed that the hiPSC-CMs aggregated into a dense, clustered structure; meanwhile, the hECs generated the micro-vessel array within the myofibers atop the printed thick construct (Fig. 3f). Similar to the phenomenon in our

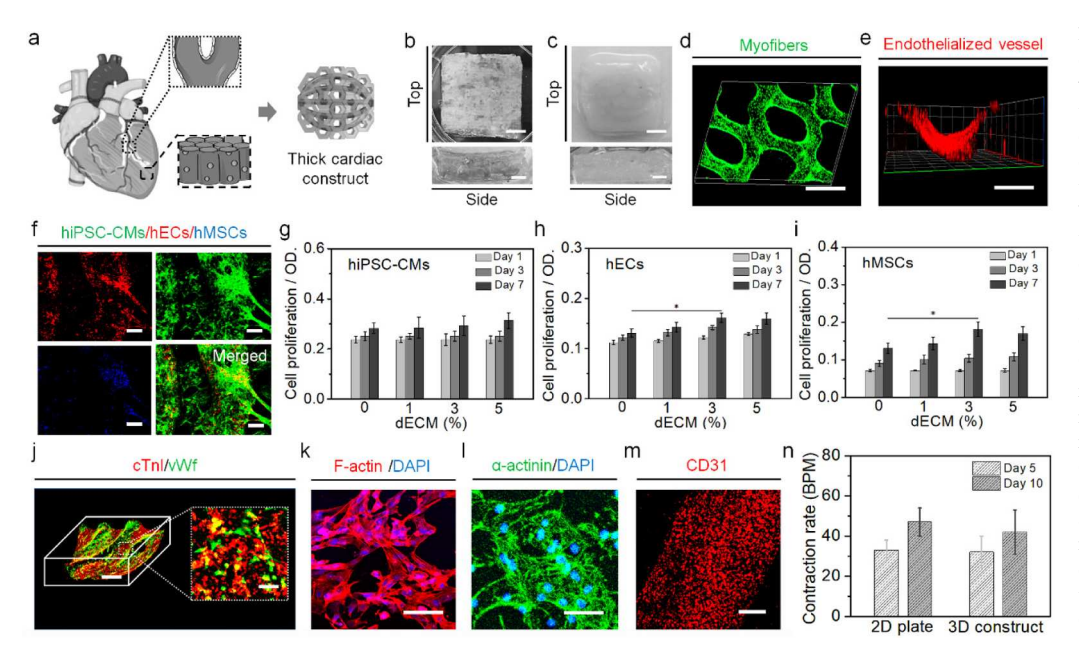


Fig. 3. Printing of a thick cellularized cardiac construct with a perfusable vasculature and in vitro characterization. (a) Schematic illustration of cardiac tissue and CAD design of our thick cardiac constructs, including anisotropic myofibers and perfusable branched vessels. (b) Photo images of the top and side views of printed thick cardiac construct. Scale bar, 5 mm (top) and 2 mm (side). (c) Photo images of a cellularized thick cardiac construct with top and side views after 7 days of culture. Scale bar (top), 5 mm. Scale bar (side), 2 mm. (d) Fluorescent images of the wave-patterned myofibers with green-colored hiPSC-CMs in the printed cardiac construct. Scale bar, 500 µm. (e) Fluorescent images of the endothelialized vessel with red-colored hECs within the cardiac constructs. Scale bar, 500 µm. (f) Distribution and organization of hiPSC-CMs (green), hMSCs (blue), and hECs (red) cocultured on the printed construct after 7 days. Scale bars, 100 μm. Cell proliferation of mono-cultured (g) hiPSC-CMs, (h) hECs, and (i) hMSCs

in the printed constructs with different ratios of the dECM fibers for 7 days (means \pm SD, $n \ge 9$, *p < 0.05). (j) 3D immunostaining image of cTnI (red) and vWf (green) within the printed construct on day 7. Scale bars, 200 μ m in the 3D image (20 μ m in 2D inset). Immunostaining (Top view) of (k) F-actin (red) and (l) α -actinin (green) of hiPSC-CMs on the printed myofiber of the cardiac construct on day 7. Scale bars, 50 μ m. (m) Immunostaining (Top view) of platelet endothelial cell adhesion molecule (CD31, red; scale bars, 250 μ m) of hECs in the printed vascular channel on day 7. (n) Beating rate of hiPSC-CMs on the 3D printed construct on day 5 and day 10 (vs. 2D well plate) (means \pm SD, $n \ge 6$). BPM, beats per minute.

previous study [14], hMSCs (blue color) became unobvious in the coculture system due to the higher density and size of hiPSC-CMs. In general, the versatility of the SL printing system in fabricating complex 3D biomimetic hierarchal architectures with micropatterns in clinically relevant dimensions was successfully demonstrated in our study. The results showed that the myofibers with anisotropic patterns were well created, while the large perfusable vasculature was generated.

To investigate the proliferation of hiPSC-CMs, hECs and hMSCs, the cells were mono-cultured on the dECM@GP hydrogels with different ratios of dECM fibers. A significant increase in the hiPSC-CM proliferation was observed over 7 days, although we did not observe a significant difference between different hydrogel groups (Fig. 3g). As shown in Fig. 3h and i, compared to the other groups, the hydrogels doped with 3 and 5 wt% dECM fibers exhibited a higher proliferation of hECs and hMSCs, suggesting the addition of dECM fibers could greatly improve cell growth of hECs and hMSCs. The increase in cell numbers also further demonstrated the cells could maintain high viability in our printed thick constructs after 7 days of culture. Additionally, a 3D immunostaining study of the myocardial contraction protein (cTnI) and the vascular protein (vWf) indicated that the cardiomyocytes were evenly distributed over the printed hexagonal patterned fibers of our thick constructs with a dense hEC network (Fig. 3j). Moreover, robust F-actin and α -actinin expression of hiPSC-CMs were identified with immunostaining on the printed constructs (Fig. 3k and 1). The organization and alignment of the sarcomeric structure were not very clear in the images due to the irregular surface of the samples. Fluorescent image analysis of the CD31 stained vessel (Top view) revealed a higher density of hEC adhesion in the printed large vessel channel (Fig. 3m). As shown in Fig. 3n, the contraction rate of the hiPSC-CMs was similar when growing on the 3Dprinted constructs and the 2D well plates after 10 days of observation. The results demonstrated that our dECM fiber-reinforced tissue constructs provided a favorable 3D matrix by combining fibrous and elastic surfaces for the resident cardiomyocytes to mimic their natural environment, which encouraged them to assume their inherent phenotype.

The heart is a mechanically active organ, so the cardiomyocyte-laden tissue constructs are subject to mechanical signals after in vivo implantation [3,57]. Several studies of biomechanical stimulation have shown that mechanical loading can profoundly affect the cytoskeletal organization and maturation of cardiomyocytes, and can thus lead to the improved excitation-contraction (E-C) coupling of grafts with the ventricle; meanwhile, shear stress also plays a significant role in angiogenesis and the maturation of microcirculation [3,58-60]. In particular, the functional maturation of the thick constructs is difficult when compared to the engineered thin tissue patches/constructs due to the limited supply of oxygen and nutrients. Therefore, we applied a customized bioreactor system containing flow and mechanical loading functions, which provides a physiologically relevant microenvironment (hydrodynamics and mechanical strain) of dual biomechanical stimulation (MS) (Fig. 4a-e). As shown in Fig. 4e, imaging confirmed the cell medium was perfused into the channel of printed branched vasculature via inlet and outlet tubes to supply the nutrients for the resident cells of thick tissue constructs. In the current design, the medium was not completely transferred through the perfusable channels when considering that the slow angiogenesis could not satisfy the requirement of nutrient supply for resident cells within thick tissue construct. Instead, the medium was transferred into the tissue constructs through the porous structure within the whole constructs. It is expected that the porous structure could also facilitate the connection of hECs in the channel with the hECs in the myofiber hydrogel.

As shown in Fig. 4f, it was observed that myocardial contractile protein (cTnI) and angiogenic protein (vWf) had a higher expression after 2 weeks of MS culture, compared to the non-stimulated controls. Additionally, the highly dense cell assemblies were evident within the constructs under MS conditions. We also observed enhanced protein expression in the dECM@GP samples, which is attributed to the improved growth of resident cells by means of the incorporated dECM fibers. Unfortunately, the images of substantial 3D sarcomeric structures could not be taken due to the limitation of the irregular surface of the

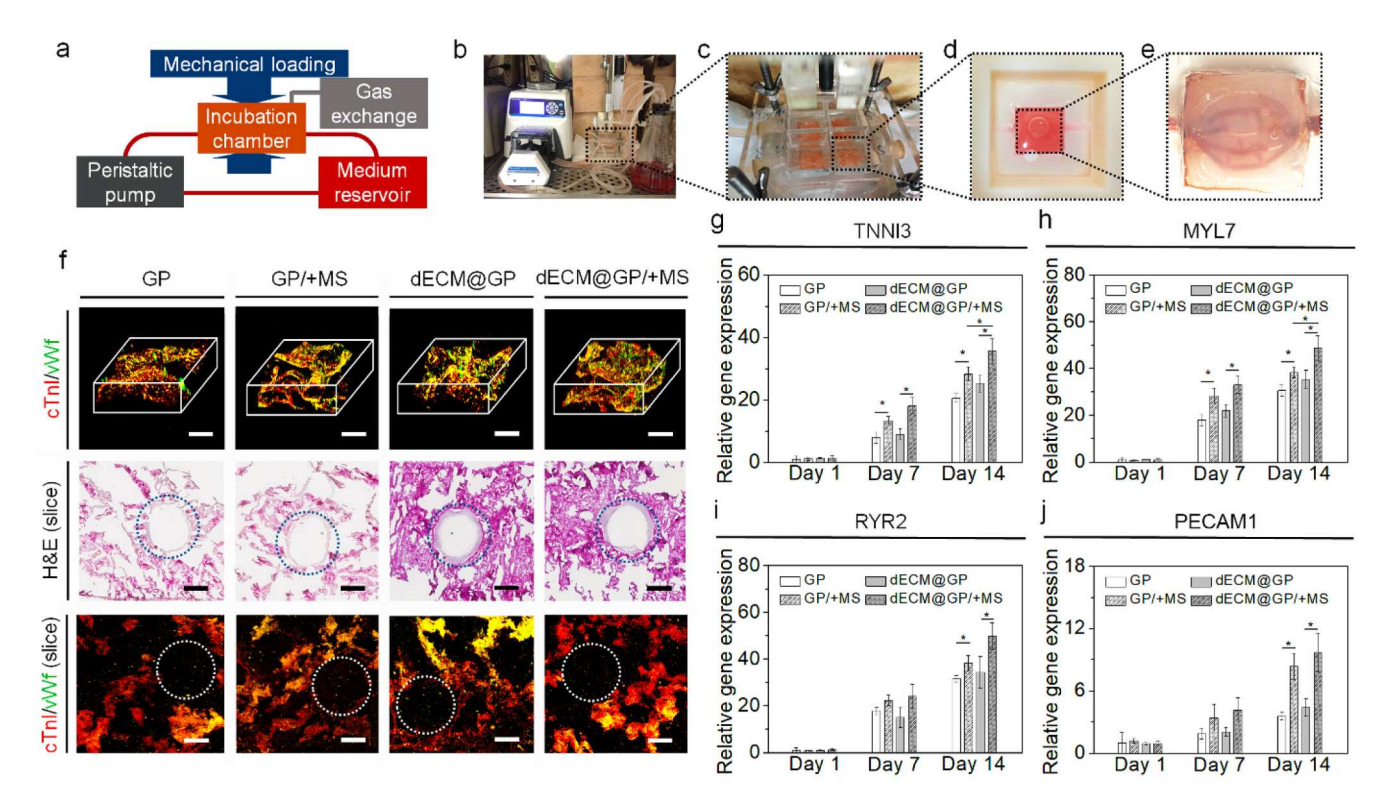


Fig. 4. Dual biomechanical stimulation (MS) culture of the cellularized constructs. (a) Schematic diagram of our customized bioreactor system that applies MS to improve the functionality of engineered thick cardiac tissue. Photo images of (b) the dual MS bioreactor culture system, (c) incubation PMMA chamber, (d) PDMS chamber holder, and (e) thick cardiac construct with a perfusable branched vasculature. (f) Immunostaining and histological images of printed cardiac constructs after 14 days of MS culture. 3D immunostaining of vWf (green) and cTnI (red) on the different constructs under MS (+MS) vs. non-stimulated conditions. Scale bars, 200 μ m. H&E staining of the slices of different constructs under MS (+MS) vs. non-stimulated conditions. Vessel channel area (blue dotted circles). Scale bars, 500 μ m. Immunostaining of the slices of different constructs with cTnI (red) and vWf (green) proteins under MS (+MS) vs. non-stimulated conditions. Vessel channel area (white dotted circles). Scale bars, 500 μ m. Gene expression of (g) myocardial contraction (TNNI3), (h) myocardial structure (MYL7), (i) E-C coupling (RYR2), and (j) angiogenesis (PECAM1) within the printed cardiac constructs under MS (+MS) vs. non-stimulated conditions (means \pm SD, $n \ge 9$, p < 0.05).

samples. Moreover, cross-sectional H&E staining further illustrated the existence of vascular channels as well as the distinct morphologic differences between GP and dECM@GP samples after a long culture period. This effectively demonstrates that compared to the loose organization of GP samples, the addition of dECM fibers enhances the structural stability of the printed hydrogel constructs. This suggests that dECM fibers can reinforce the mechanical strength of the printed constructs, and thereby improve the endurance of external forces during the repeatable stretching cycles against material deformation in the MS condition. However, there is no observable difference between the stimulated and non-stimulated samples with cross-sectional immunostaining imaging. It was thought that the cells were encapsulated in the thick constructs; however, the slices were too thin to clearly distinguish the cell morphology and distribution from the hydrogel samples. Moreover, the CD31 stained hECs in the channels were clearly not observed in the cross-sectional images, which were also attributed to the thin slices. Therefore, in future study, we need to find proper characterization methods to better analyze the samples when considering the limitation of the current methods for the large, thick samples. Generally, the dECM fiber-reinforced constructs were capable of tolerating the cyclic stretching and continuous perfusion in a physiologically relevant environment as compared to the control group (GP constructs). As the surface of thick constructs became irregular after 2 weeks of culture, we failed to collect the data of cellular contraction and high magnification

Moreover, gene expression was measured to quantitatively evaluate the development of thick tissue constructs. It was observed that all cardiac-related genes were considerably increased over time, suggesting an obvious increase in the functional improvement of the hiPSC-CMs and hECs on the printed thick constructs. More importantly, compared to other control groups, the expression of the TNNI3 gene of cells growing on the dECM@GP samples was significantly upregulated on day 14 under the MS condition (Fig. 4g). Meanwhile, the expression of the MYL7 gene on cells growing on the dECM@GP samples also assumed a similar profile (Fig. 4h). In addition, as compared to the non-stimulated control, the increased expression of the RYR2 gene was also observed under the MS condition on day 14, further demonstrating that the application of MS could enhance contractile and electrical functionalities of iPSC-CMs (Fig. 4i). Moreover, the expression of the angiogenic PECAM1 gene had an average of 3-fold increase under MS condition on day 14 compared to the non-stimulated control, due to the dynamic perfusion culture (Fig. 4j). The results confirmed that the MS culture provided cardiogenic cells with sequences of hemodynamic and electromechanical signals, and thus effectively recapitulated the physiological functionality of the cardiac niche necessary for improving myocardial functionality. Compared to the role of dECMs, the effect of MS culture on cell functionality was more evident according to the gene expression results. These results suggested that the material properties of constructs could improve biological activity while the effect of the MS culture on cell functions was more significant. Therefore, it is necessary that the MS culture is used to enhance the functionality of thick myocardial constructs.

This study introduces a new method for fabricating clinically relevant cardiac constructs with a precise microstructure of anisotropic myofibers and perfusable vascular channels, using a customized beam-scanning SL printing technique. Superior to extrusion-based 3D bioprinting, this technique is not limited by bioink composition (such as hybrid size and viscosity) and allows for easy achievement of high-

resolution manufacturing. For future studies, it is essential to gather substantial and robust evidence, such as advanced analysis and large animal implantation, to demonstrate the advantages of our design. Regarding the immunology of the decellularized porcine tissue for clinical translation, previous research has shown that the decellularization process can reduce the immune responses of ECMs compared to xenogeneic tissue [40,61]. Alternatively, the use of immunodeficient pigs could help mitigate this concern. While our current study on thick tissue products may be limited by effective analysis methods, it presents a potential methodology for manufacturing clinically relevant products in future studies. This approach holds promise for addressing the challenges of regenerating complex human tissues/organs and engineering in vitro disease models effectively.

4. Conclusion

In this study, a novel engineered myocardial construct with anisotropic myofibers and branched perfusable vascular channels at clinically relevant dimensions was successfully developed using a beam-scanning SL printing. Our aim was to replicate the native characteristics of the human heart, with the ultimate goal of repairing the MI-damaged myocardium and restoring its functionality. To assist the precise manufacturing of a hierarchical microstructure in SL printing, a tissuespecific bioink was tailored by dispersed dECM microfibers of myocardial tissue into photocrosslinkable ink solution, which not only maintained the fibrous structure of the native cardiac ECM, but also enhanced the tunable mechanical moduli and bioactivity of the printed constructs. This study tries to address some major challenges faced in engineered clinically relevant cardiac tissues, including the incorporation of advanced structural characteristics, a biomimetic matrix environment, and physiologically relevant biomechanical cues. These developments hold immense potential for effectively repairing damaged human myocardial tissues, and treating MI-related cardiovascular diseases.

CRediT authorship contribution statement

Haitao Cui: Conceptualization, Data curation, Formal analysis, Investigation, Methodology, Validation, Visualization, Writing – original draft. Zu-Xi Yu: Data curation, Formal analysis, Investigation, Methodology, Resources, Validation. Yimin Huang: Conceptualization, Data curation, Investigation, Visualization, Writing – review & editing. Sung Yun Hann: Investigation, Methodology. Timothy Esworthy: Writing – review & editing. Yin-Lin Shen: Writing – review & editing. Lijie Grace Zhang: Conceptualization, Funding acquisition, Project administration, Supervision, Writing – review & editing.

Declaration of competing interest

The authors declare the following financial interests/personal relationships which may be considered as potential competing interests: Lijie Grace Zhang reports financial support was provided by American Heart Association. Lijie Grace Zhang reports financial support was provided by National Science Foundation. Lijie Grace Zhang has patent pending to The George Washington University.

Data availability

Data will be made available on request.

Acknowledgements

The authors would like to thank Dr. Chengyu Liu and the iPSC Core at NHLBI for providing hiPSC-CMs and culture protocol. The authors also thank GWU Image Center for microscopy and image analysis.

Funding sources

This work was supported by the American Heart Association Transformative Project Award, and NSF EBMS Program Grant 1856321.

References

- [1] T.A. Ghebreyesus, Word Health Statistics 2022, Word Health Organization, Switzerland, 2022
- [2] H. Hashimoto, E.N. Olson, R. Bassel-Duby, Therapeutic approaches for cardiac regeneration and repair, Nat. Rev. Cardiol. 15 (10) (2018) 585–600, https://doi. org/10.1038/s41569-018-0036-6.
- [3] H. Parsa, K. Ronaldson, G. Vunjak-Novakovic, Bioengineering methods for myocardial regeneration, Adv. Drug Deliv. Rev. 96 (2016) 195–202, https://doi. org/10.1016/j.addr.2015.06.012.
- [4] M.Y. Emmert, R.W. Hitchcock, S.P. Hoerstrup, Cell therapy, 3D culture systems and tissue engineering for cardiac regeneration, Adv. Drug Deliv. Rev. 69-70 (2014) 254–269, https://doi.org/10.1016/j.addr.2013.12.004.
- [5] J. Zhang, W. Zhu, M. Radisic, G. Vunjak-Novakovic, Can we engineer a human cardiac patch for therapy? Circ. Res. 123 (2) (2018) 244–265, https://doi.org/ 10.1161/CIRCRESAHA.118.311213.
- [6] F. Weinberger, I. Mannhardt, T. Eschenhagen, Engineering cardiac muscle tissue: a maturating field of research, Circ. Res. 120 (9) (2017) 1487–1500, https://doi.org/ 10.1161/CIRCRESAHA.117.310738.
- [7] W.H. Zimmermann, Tissue engineered heart repair from preclinical models to firstin-patient studies, Curr. Opin. Physiol. 14 (2020) 70–77, https://doi.org/10.1016/ j.cophys.2020.02.001.
- [8] Y. Efraim, H. Sarig, N. Cohen Anavy, U. Sarig, E. de Berardinis, S.Y. Chaw, M. Krishnamoorthi, J. Kalifa, H. Bogireddi, T.V. Duc, T. Kofidis, L. Baruch, F. Y. Boey, S.S. Venkatraman, M. Machluf, Biohybrid cardiac ECM-based hydrogels improve long term cardiac function post myocardial infarction, Acta Biomater. 50 (2017) 220–233, https://doi.org/10.1016/j.actbio.2016.12.015.
- [9] J. Jang, H.J. Park, S.W. Kim, H. Kim, J.Y. Park, S.J. Na, H.J. Kim, M.N. Park, S. H. Choi, S.H. Park, S.W. Kim, S.M. Kwon, P.J. Kim, D.W. Cho, 3D printed complex tissue construct using stem cell-laden decellularized extracellular matrix bioinks for cardiac repair, Biomaterials 112 (2017) 264–274, https://doi.org/10.1016/j.biomaterials.2016.10.026.
- [10] N.Y. Liaw, W.H. Zimmermann, Mechanical stimulation in the engineering of heart muscle, Adv. Drug Deliv. Rev. 96 (2016) 156–160, https://doi.org/10.1016/j. addr.2015.09.001.
- [11] F. Weinberger, K. Breckwoldt, S. Pecha, A. Kelly, B. Geertz, J. Starbatty, T. Yorgan, K.H. Cheng, K. Lessmann, T. Stolen, M. Scherrer-Crosbie, G. Smith, H. Reichenspurner, A. Hansen, T. Eschenhagen, Cardiac repair in guinea pigs with human engineered heart tissue from induced pluripotent stem cells, Sci. Transl. Med. 8 (363) (2016) 363ra148, https://doi.org/10.1126/scitranslmed.aaf8781.
- [12] A. Wnorowski, J.C. Wu, 3-dimensionally printed, native-like scaffolds for myocardial tissue engineering, Circ. Res. 120 (8) (2017) 1224–1226, https://doi. org/10.1161/CIRCRESAHA.117.310862.
- [13] K. Huang, E.W. Ozpinar, T. Su, J. Tang, D. Shen, L. Qiao, S. Hu, Z. Li, H. Liang, K. Mathews, V. Scharf, D.O. Freytes, K. Cheng, An off-the-shelf artificial cardiac patch improves cardiac repair after myocardial infarction in rats and pigs, Sci. Transl. Med. 12 (538) (2020), https://doi.org/10.1126/scitranslmed.aat9683.
- [14] H. Cui, C. Liu, T. Esworthy, Y. Huang, Z.X. Yu, X. Zhou, H. San, S.J. Lee, S.Y. Hann, M. Boehm, M. Mohiuddin, J.P. Fisher, L.G. Zhang, 4D physiologically adaptable cardiac patch: a 4-month in vivo study for the treatment of myocardial infarction, Sci. Adv. 6 (26) (2020) eabb5067, https://doi.org/10.1126/sciadv.abb5067.
- [15] Y. Wang, H. Cui, Y. Wang, C. Xu, T.J. Esworthy, S.Y. Hann, M. Boehm, Y.L. Shen, D. Mei, L.G. Zhang, 4D printed cardiac construct with aligned myofibers and adjustable curvature for myocardial regeneration, ACS Appl. Mater. Interfaces 13 (11) (2021) 12746–12758, https://doi.org/10.1021/acsami.0c17610.
- [16] S. Miao, H. Cui, M. Nowicki, S.J. Lee, J. Almeida, X. Zhou, W. Zhu, X. Yao, F. Masood, M.W. Plesniak, M. Mohiuddin, L.G. Zhang, Photolithographic-stereolithographic-tandem fabrication of 4D smart scaffolds for improved stem cell cardiomyogenic differentiation, Biofabrication 10 (3) (2018), 035007, https://doi.org/10.1088/1758-5090/aabe0b.
- [17] C. Beans, Inner workings: the race to patch the human heart, Proc. Natl. Acad. Sci. U. S. A. 115 (26) (2018) 6518–6520, https://doi.org/10.1073/pnas.1808317115.
- [18] S. Fleischer, A. Shapira, R. Feiner, T. Dvir, Modular assembly of thick multifunctional cardiac patches, Proc. Natl. Acad. Sci. U. S. A. 114 (8) (2017) 1898–1903, https://doi.org/10.1073/pnas.1615728114.
- [19] H. Cui, S. Miao, T. Esworthy, X. Zhou, S.J. Lee, C. Liu, Z.X. Yu, J.P. Fisher, M. Mohiuddin, L.G. Zhang, 3D bioprinting for cardiovascular regeneration and pharmacology, Adv. Drug Deliv. Rev. 132 (2018) 252–269, https://doi.org/ 10.1016/j.addr.2018.07.014.
- [20] A. Lee, A.R. Hudson, D.J. Shiwarski, J.W. Tashman, T.J. Hinton, S. Yerneni, J. M. Bliley, P.G. Campbell, A.W. Feinberg, 3D bioprinting of collagen to rebuild components of the human heart, Science 365 (6452) (2019) 482–487, https://doi.org/10.1126/science.aav9051.
- [21] H. Cui, M. Nowicki, J.P. Fisher, L.G. Zhang, 3D bioprinting for organ regeneration, Adv. Healthc. Mater. 6 (1) (2017) 1601118, https://doi.org/10.1002/ adhm.201601118.
- [22] S.Y. Hann, H. Cui, T. Esworthy, S. Miao, X. Zhou, S.J. Lee, J.P. Fisher, L.G. Zhang, Recent advances in 3D printing: vascular network for tissue and organ

- regeneration, Transl. Res. 211 (2019) 46–63, https://doi.org/10.1016/j.
- [23] N.J. Castro, W. Zhu, H.T. Cui, S.J. Lee, L.G. Zhang, 3D bioprinting for regenerative engineering, in: Regenerative Engineering: Advanced Materials Science Principles, 2018, pp. 119–137.
- [24] H. Cui, W. Zhu, Y. Huang, C. Liu, Z.X. Yu, M. Nowicki, S. Miao, Y. Cheng, X. Zhou, S.J. Lee, Y. Zhou, S. Wang, M. Mohiuddin, K. Horvath, L.G. Zhang, In vitro and in vivo evaluation of 3D bioprinted small-diameter vasculature with smooth muscle and endothelium, Biofabrication 12 (1) (2019), 015004, https://doi.org/10.1088/1758-5090/ab402c.
- [25] Q. Gao, Z.J. Liu, Z.W. Lin, J.J. Qiu, Y. Liu, A. Liu, Y.D. Wang, M.X. Xiang, B. Chen, J.Z. Fu, Y. He, 3D bioprinting of vessel-like structures with multilevel fluidic channels, ACS Biomater. Sci. Eng. 3 (3) (2017) 399–408, https://doi.org/10.1021/acsbiomaterials.6b00643.
- [26] W. Jia, P.S. Gungor-Ozkerim, Y.S. Zhang, K. Yue, K. Zhu, W. Liu, Q. Pi, B. Byambaa, M.R. Dokmeci, S.R. Shin, A. Khademhosseini, Direct 3D bioprinting of perfusable vascular constructs using a blend bioink, Biomaterials 106 (2016) 58–68, https:// doi.org/10.1016/j.biomaterials.2016.07.038.
- [27] H. Cui, W. Zhu, M. Nowicki, X. Zhou, A. Khademhosseini, L.G. Zhang, Hierarchical fabrication of engineered vascularized bone biphasic constructs via dual 3D bioprinting: integrating regional bioactive factors into architectural design, Adv. Healthc. Mater. 5 (17) (2016) 2174–2181, https://doi.org/10.1002/ adhm.201600505.
- [28] D.B. Kolesky, K.A. Homan, M.A. Skylar-Scott, J.A. Lewis, Three-dimensional bioprinting of thick vascularized tissues, Proc. Natl. Acad. Sci. U. S. A. 113 (12) (2016) 3179–3184, https://doi.org/10.1073/pnas.1521342113.
- [29] S.Y. Hann, H. Cui, T. Esworthy, X. Zhou, S.J. Lee, M.W. Plesniak, L.G. Zhang, Dual 3D printing for vascularized bone tissue regeneration, Acta Biomater. 123 (2021) 263–274, https://doi.org/10.1016/j.actbio.2021.01.012.
- [30] H. Cui, T. Esworthy, X. Zhou, S.Y. Hann, R.I. Glazer, R. Li, L.G. Zhang, Engineering a novel 3D printed vascularized tissue model for investigating breast cancer metastasis to bone, Adv. Healthc. Mater. 9 (15) (2020), e1900924, https://doi.org/ 10.1002/adhm.201900924.
- [31] S. Miao, H. Cui, M. Nowicki, L. Xia, X. Zhou, S.J. Lee, W. Zhu, K. Sarkar, Z. Zhang, L.G. Zhang, Stereolithographic 4D bioprinting of multiresponsive architectures for neural engineering, Adv. Biosyst. 2 (9) (2018) 1800101, https://doi.org/10.1002/ advis-030000103
- [32] X. Zhou, S. Tenaglio, T. Esworthy, S.Y. Hann, H. Cui, T.J. Webster, H. Fenniri, L. G. Zhang, Three-dimensional printing biologically inspired DNA-based gradient scaffolds for cartilage tissue regeneration, ACS Appl. Mater. Interfaces 12 (29) (2020) 33219–33228, https://doi.org/10.1021/acsami.0c07918.
- [33] T. Agarwal, G.M. Fortunato, S.Y. Hann, B. Ayan, K.Y. Vajanthri, D. Presutti, H. Cui, A.H.P. Chan, M. Costantini, V. Onesto, C. Di Natale, N.F. Huang, P. Makvandi, M. Shabani, T.K. Maiti, L.G. Zhang, C. De Maria, Recent advances in bioprinting technologies for engineering cardiac tissue, Mater. Sci. Eng. C Mater. Biol. Appl. 124 (2021), 112057. https://doi.org/10.1016/j.msec.2021.112057.
- [34] T. Agarwal, S.Y. Hann, I. Chiesa, H. Cui, N. Celikkin, S. Micalizzi, A. Barbetta, M. Costantini, T. Esworthy, L.G. Zhang, C. De Maria, T.K. Maiti, 4D printing in biomedical applications: emerging trends and technologies, J. Mater. Chem. B 9 (32) (2021) 7608–7632. https://doi.org/10.1039/d1tb01335a
- [35] S. Miao, N. Castro, M. Nowicki, L. Xia, H. Cui, X. Zhou, W. Zhu, S.J. Lee, K. Sarkar, G. Vozzi, Y. Tabata, J. Fisher, L.G. Zhang, 4D printing of polymeric materials for tissue and organ regeneration, Mater. Today (Kidlington) 20 (10) (2017) 577–591, https://doi.org/10.1016/j.mattod.2017.06.005.
- [36] B.S. Kim, S. Das, J. Jang, D.W. Cho, Decellularized extracellular matrix-based bioinks for engineering tissue- and organ-specific microenvironments, Chem. Rev. 120 (19) (2020) 10608–10661, https://doi.org/10.1021/acs.chemrev.9b00808.
 [37] M. Brown, J. Li, C. Moraes, M. Tabrizian, N.Y.K. Li-Jessen, Decellularized
- [37] M. Brown, J. Li, C. Moraes, M. Tabrizian, N.Y.K. Li-Jessen, Decellularized extracellular matrix: new promising and challenging biomaterials for regenerative medicine, Biomaterials 289 (2022), 121786, https://doi.org/10.1016/j. biomaterials.2022.121786.
- [38] X. Zhang, X. Chen, H. Hong, R. Hu, J. Liu, C. Liu, Decellularized extracellular matrix scaffolds: recent trends and emerging strategies in tissue engineering, Bioact. Mater. 10 (2022) 15–31, https://doi.org/10.1016/j. bioactmat.2021.09.014.
- [39] D. Bejleri, M.E. Davis, Decellularized extracellular matrix materials for cardiac repair and regeneration, Adv. Healthc. Mater. 8 (5) (2019), e1801217, https://doi. org/10.1002/adhm.201801217.
- [40] F. Pati, J. Jang, D.H. Ha, S. Won Kim, J.W. Rhie, J.H. Shim, D.H. Kim, D.W. Cho, Printing three-dimensional tissue analogues with decellularized extracellular matrix bioink, Nat. Commun. 5 (2014) 3935, https://doi.org/10.1038/ ncomms4935
- [41] Y.J. Shin, R.T. Shafranek, J.H. Tsui, J. Walcott, A. Nelson, D.H. Kim, 3D bioprinting of mechanically tuned bioinks derived from cardiac decellularized extracellular matrix, Acta Biomater. 119 (2021) 75–88, https://doi.org/10.1016/j. actbio.2020.11.006.
- [42] L. Pang, Toxicity testing in the era of induced pluripotent stem cells: a perspective regarding the use of patient-specific induced pluripotent stem cell-derived

- cardiomyocytes for cardiac safety evaluation, Curr. Opin. Toxicol. 23-24 (2020) 50–55, https://doi.org/10.1016/j.cotox.2020.04.001.
- [43] L. Barad, R. Schick, N. Zeevi-Levin, J. Itskovitz-Eldor, O. Binah, Human embryonic stem cells vs human induced pluripotent stem cells for cardiac repair, Can. J. Cardiol. 30 (11) (2014) 1279–1287, https://doi.org/10.1016/j.cjca.2014.06.023.
- [44] T. Eschenhagen, K. Ridders, F. Weinberger, How to repair a broken heart with pluripotent stem cell-derived cardiomyocytes, J. Mol. Cell. Cardiol. 163 (2022) 106–117, https://doi.org/10.1016/j.yjmcc.2021.10.005.
- [45] L. Gao, Z.R. Gregorich, W. Zhu, S. Mattapally, Y. Oduk, X. Lou, R. Kannappan, A. V. Borovjagin, G.P. Walcott, A.E. Pollard, V.G. Fast, X. Hu, S.G. Lloyd, Y. Ge, J. Zhang, Large cardiac muscle patches engineered from human induced-pluripotent stem cell-derived cardiac cells improve recovery from myocardial infarction in swine, Circulation 137 (16) (2018) 1712–1730, https://doi.org/10.1161/CIRCULATIONAHA.117.030785.
- [46] Y. Lin, K.L. Linask, B. Mallon, K. Johnson, M. Klein, J. Beers, W. Xie, Y. Du, C. Liu, Y. Lai, J. Zou, M. Haigney, H. Yang, M. Rao, G. Chen, Heparin promotes cardiac differentiation of human pluripotent stem cells in chemically defined albumin-free medium, enabling consistent manufacture of cardiomyocytes, Stem Cells Transl. Med. 6 (2) (2017) 527–538, https://doi.org/10.5966/sctm.2015-0428.
- [47] P. Zhou, W.T. Pu, Recounting cardiac cellular composition, Circ. Res. 118 (3) (2016) 368–370, https://doi.org/10.1161/CIRCRESAHA.116.308139.
- [48] A.R. Pinto, A. Ilinykh, M.J. Ivey, J.T. Kuwabara, M.L. D'Antoni, R. Debuque, A. Chandran, L. Wang, K. Arora, N.A. Rosenthal, M.D. Tallquist, Revisiting cardiac cellular composition, Circ. Res. 118 (3) (2016) 400–409, https://doi.org/10.1161/ CIRCRESAHA.115.307778.
- [49] S. Lehoux, A. Tedgui, Cellular mechanics and gene expression in blood vessels, J. Biomech. 36 (5) (2003) 631–643, https://doi.org/10.1016/s0021-9290(02) 00441-4
- [50] C. Yu, X. Ma, W. Zhu, P. Wang, K.L. Miller, J. Stupin, A. Koroleva-Maharajh, A. Hairabedian, S. Chen, Scanningless and continuous 3D bioprinting of human tissues with decellularized extracellular matrix, Biomaterials 194 (2019) 1–13, https://doi.org/10.1016/j.biomaterials.2018.12.009.
- [51] T. Jiao, R.J. Clifton, G.L. Converse, R.A. Hopkins, Measurements of the effects of decellularization on viscoelastic properties of tissues in ovine, baboon, and human heart valves, Tissue Eng. Part A 18 (3–4) (2012) 423–431, https://doi.org/ 10.1089/ten.TEA.2010.0677.
- [52] J.M. Lee, S.L. Sing, E.Y.S. Tan, W.Y. Yeong, Bioprinting in cardiovascular tissue engineering: a review, Int. J. Bioprinting 2 (2) (2016) 27–36, https://doi.org/ 10.18063/lib.2016.02.006.
- [53] D. Rohmer, A. Sitek, G.T. Gullberg, Reconstruction and visualization of fiber and laminar structure in the normal human heart from ex vivo diffusion tensor magnetic resonance imaging (DTMRI) data, Investig. Radiol. 42 (11) (2007) 777-789, https://doi.org/10.1097/RII.0b013e3181238330.
- [54] F. Pashakhanloo, D.A. Herzka, H. Ashikaga, S. Mori, N. Gai, D.A. Bluemke, N. A. Trayanova, E.R. McVeigh, Myofiber architecture of the human atria as revealed by submillimeter diffusion tensor imaging, Circ. Arrhythm. Electrophysiol. 9 (4) (2016), e004133, https://doi.org/10.1161/CIRCEP.116.004133.
- [55] D.A. Narmoneva, R. Vukmirovic, M.E. Davis, R.D. Kamm, R.T. Lee, Endothelial cells promote cardiac myocyte survival and spatial reorganization: implications for cardiac regeneration, Circulation 110 (8) (2004) 962–968, https://doi.org/ 10.1161/01.CIR.0000140667.37070.07.
- [56] R.J. Dilley, W.A. Morrison, Vascularisation to improve translational potential of tissue engineering systems for cardiac repair, Int. J. Biochem. Cell Biol. 56 (2014) 38–46. https://doi.org/10.1016/j.biocel.2014.10.020.
- [57] K.L. Coulombe, V.K. Bajpai, S.T. Andreadis, C.E. Murry, Heart regeneration with engineered myocardial tissue, Annu. Rev. Biomed. Eng. 16 (2014) 1–28, https://doi.org/10.1146/annurev-bioeng-071812-152344.
- [58] P.H. Nguyen, S.F. Coquis-Knezek, M.W. Mohiuddin, E. Tuzun, C.M. Quick, The complex distribution of arterial system mechanical properties, pulsatile hemodynamics, and vascular stresses emerges from three simple adaptive rules, Am. J. Physiol. Heart Circ. Physiol. 308 (5) (2015) H407–H415, https://doi.org/10.1152/aipheart.00537.2014.
- [59] M.E. McCormick, E. Tzima, Pulling on my heartstrings: mechanotransduction in cardiac development and function, Curr. Opin. Hematol. 23 (3) (2016) 235–242, https://doi.org/10.1097/MOH.000000000000240.
- [60] A.P. Antoniadis, P. Mortier, G. Kassab, G. Dubini, N. Foin, Y. Murasato, A. A. Giannopoulos, S. Tu, K. Iwasaki, Y. Hikichi, F. Migliavacca, C. Chiastra, J. J. Wentzel, F. Gijsen, J.H. Reiber, P. Barlis, P.W. Serruys, D.L. Bhatt, G. Stankovic, E.R. Edelman, G.D. Giannoglou, Y. Louvard, Y.S. Chatzizisis, Biomechanical modeling to improve coronary artery bifurcation stenting: expert review document on techniques and clinical implementation, JACC Cardiovasc. Interv. 8 (10) (2015) 1281–1296, https://doi.org/10.1016/j.jcin.2015.06.015.
- [61] F. Boccafoschi, M. Botta, L. Fusaro, F. Copes, M. Ramella, M. Cannas, Decellularized biological matrices: an interesting approach for cardiovascular tissue repair and regeneration, J. Tissue Eng. Regen. Med. 11 (5) (2017) 1648–1657, https://doi.org/10.1002/term.2103.